

Scalable Heterogeneous Graph Foundation Models for Data-Driven Optimal Power Flow in Smart Grids

Massimiliano Lupo Pasini, Yijiang Li, Kibaek Kim, and Teja Kuruganti

Abstract—Fast and reliable optimal power flow (OPF) approximation is essential for reliable smart-grid operation, yet many learning-based surrogates either flatten the native heterogeneous structure of power networks, target a limited set of grid topologies, or lack scalable infrastructure for graph foundation models (GFMs) training. This paper presents a scalable heterogeneous graph neural network (GNN) workflow, built on HydraGNN, for data-driven OPF surrogate modeling and OPF-GFM development. The workflow preserves the distinct node and edge types of power grids—buses, generators, loads, shunts, AC lines, transformers, and device-to-bus couplings—and supports distributed preprocessing, training, hyperparameter optimization (HPO), and downstream fine-tuning on leadership-class supercomputers. Using three million heterogeneous graph instances spanning ten PGLib-OPF cases, from 14 to 13,659 buses, we conduct DeepHyper-driven HPO on the ORNL Frontier supercomputer. The campaign identifies compact models (~1.6–1.7M parameters) with the lowest validation losses. Downstream experiments on feasibility classification and $N-1$ contingency regression show that fine-tuning pretrained OPF GFMs improves low-data accuracy, stabilizes training, accelerates convergence, and reduces adaptation cost when partial or head-only fine-tuning is used.

Index Terms—Optimal power flow, smart grid, graph neural networks, heterogeneous graphs, graph foundation models, physics-informed machine learning, distributed training, hyperparameter optimization.

I. INTRODUCTION

OPTIMAL power flow (OPF) is a fundamental computational primitive for power-grid operation, planning, and decision support [1], [2]. Given a grid topology, component parameters, generator capabilities, and load demands, the alternating current OPF (AC-OPF) problem seeks a feasible operating point that minimizes generation cost while satisfying voltage, current, power-flow, and equipment constraints. The

solution contains bus voltage magnitudes and voltage angles, from which additional electrical quantities such as branch flows, currents, and losses can be derived.

Modern smart grids increasingly involve heterogeneous devices, frequent changes in operating conditions, distributed and controllable resources, topology variations, and the need for fast decision support. These trends motivate learning-based OPF surrogates that can approximate OPF solutions with low latency. Prior work has explored imitation-learning graph neural networks (GNNs) for OPF approximation [3], topology-aware GNNs for feasible and adaptive AC-OPF prediction [4], neural architectures derived from iterative AC-OPF algorithms [5], GNN-assisted solver initialization [6], and physics-informed neural approaches that embed AC-OPF constraints into training [7]. Recent studies have further introduced heterogeneous graph representations and attention mechanisms for AC-OPF [8]–[10], while LUMINA and LUMINA-Bench have advanced foundation-model-style AC-OPF learning through topology transfer, feasibility-aware objectives, standardized benchmarks, zero-shot generalization, and fine-tuning protocols [11]–[13].

These efforts show the promise of graph-based OPF learning, but they leave open a complementary systems question: how to scale heterogeneous OPF GFM training, architecture selection, and downstream adaptation to the full diversity and volume of available OPF data on leadership-class computing platforms. Existing benchmark-oriented studies provide controlled comparisons across architectures, losses, transfer settings, and feasibility metrics, but full-corpus distributed preprocessing, large-scale multi-architecture HPO, and downstream fine-tuning introduce additional challenges in memory footprint, communication cost, data loading, and training stability.

This paper addresses that systems-scale gap by developing a scalable heterogeneous GNN workflow in HydraGNN¹ [14] for OPF surrogate modeling and GFM training. The central objective is to build an OPF GFM: a single heterogeneous GNN pretrained on a broad distribution of grid topologies, demand profiles, generation mixes, and operating conditions, whose learned representations transfer across grid families and sizes and can be fine-tuned to downstream OPF tasks with fewer labeled solutions than training topology-specific surrogates from scratch.

The main contributions of this paper are as follows:

M. Lupo Pasini and T. Kuruganti are with the Computational Sciences and Engineering Division, Oak Ridge National Laboratory, 1 Bethel Valley Road, Oak Ridge, TN 37831, USA.

Y. Li and K. Kim are with the Mathematics and Computer Science Division, Argonne National Laboratory, 9700 S. Cass Avenue, Lemont, IL 60439.

Manuscript received Month XX, 2026; revised Month XX, 2026.

This manuscript has been authored in part by UT-Battelle, LLC, under contract DE-AC05-00OR22725 with the US Department of Energy (DOE). The US government retains and the publisher, by accepting the article for publication, acknowledges that the US government retains a nonexclusive, paid-up, irrevocable, worldwide license to publish or reproduce the published form of this manuscript, or allow others to do so, for US government purposes. DOE will provide public access to these results of federally sponsored research in accordance with the DOE Public Access Plan (<http://energy.gov/downloads/doe-public-access-plan>). This research used resources of the Oak Ridge Leadership Computing Facility at Oak Ridge National Laboratory, which is supported by the Office of Science of the U.S. Department of Energy under Contract No. DE-AC05-00OR22725.

¹<https://github.com/ORNL/HydraGNN>

- We extend HydraGNN with scalable heterogeneous graph learning support for OPF, including node-type-specific input embeddings, relation-specific message passing, variable edge-attribute dimensions, heterogeneous pooling, graph-attribute conditioning, and node-type-specific prediction heads.
- We construct a distributed preprocessing and HDF5 data pipeline for the full ten-case OPF corpus, comprising approximately three million heterogeneous graph instances spanning grids from 14 to 13,659 buses.
- We perform Frontier-scale HPO with DeepHyper across six heterogeneous GNN architectures on the full multi-case dataset, yielding 153 valid trials and identifying HeteroSAGE and HeteroHEAT as the most accurate and compact architectures.
- We develop and evaluate a pretraining and fine-tuning protocol for OPF GFM, demonstrating downstream adaptation to OPF feasibility classification and $N-1$ contingency regression.

Table I summarizes how the proposed workflow differs from typical prior GNN-based OPF surrogate modeling approaches.

II. RELATED WORK ON LEARNING-BASED AC-OPF SURROGATES

A. GNN-Based AC-OPF Surrogates

GNNs are a natural model class for OPF because power-system topology directly determines the coupling among buses, generators, loads, and branches. Early GNN-based OPF work formulated OPF approximation as an imitation-learning problem over graph-structured grid data [3]. Subsequent topology-aware approaches exploited structural locality in AC-OPF quantities to improve feasibility and adaptation under topology changes [4]. In this context, an OPF prediction is considered feasible if the predicted grid state satisfies voltage, angle, generator, thermal-flow, and power-balance constraints for the given topology and operating condition, within prescribed engineering tolerances. Other approaches have used graph-based neural models to emulate or accelerate iterative solver behavior, including directed-acyclic neural architectures derived from Newton-Raphson-style AC-OPF solution maps [5] and GNN-based initial estimates designed to improve interior-point solver convergence [6]. These studies establish GNNs as effective OPF surrogates, but many are centered on a specific architecture, training regime, or fixed set of grid cases.

B. Feasibility-Aware and Physics-Informed OPF Learning

A central challenge in learning OPF surrogates is that low prediction error does not automatically imply physical feasibility. Physics-informed neural OPF formulations therefore incorporate AC power-flow equations, feasibility penalties, or constraint residuals into the training process [7]. Related feasibility-aware GNN approaches penalize voltage, line-flow, or power-balance violations during training and evaluate models not only by prediction error but also by constraint satisfaction [8]. Lagrangian and augmented-Lagrangian losses have also been used to balance accuracy and feasibility by adaptively weighting constraint violations.

C. Heterogeneous Graph Representations for Power Systems

Power systems contain multiple physical component types, including buses, generators, loads, shunts, lines, transformers, and device-to-bus couplings. Homogeneous graph representations can obscure these distinctions by treating all nodes and edges uniformly. Recent OPF-GNN studies have therefore begun to use heterogeneous graph representations that explicitly encode component and relation types. OPF-HGNN proposes a heterogeneous GNN formulation with differentiable grid-constraint penalties for AC-OPF generalization [8]. Other studies investigate attention-based heterogeneous graph mechanisms for AC-OPF [9] and local/global heterogeneous message passing for AC-OPF solutions [10]. More broadly, heterogeneous OPF models build on established message-passing and graph-transformer layers, including GraphSAGE [15], graph attention [16], GATv2 [17], principal neighborhood aggregation [18], heterogeneous graph transformers [19], and heterogeneous edge-enhanced attention [20].

D. Grid Foundation Models, LUMINA, and Scalable Model Selection

Recent work has begun to move from topology-specific OPF surrogates toward grid foundation models that learn reusable representations across multiple power-system configurations. LUMINA formulates AC-OPF surrogate learning as a GFM for constrained scientific systems, emphasizing topology transfer, feasibility-aware learning, and reliability under distribution shift [11]. It studies homogeneous and heterogeneous GNN architectures, supervised and constraint-aware objectives, zero-shot transfer, fine-tuning, and hard-regime behavior across AC-OPF cases. LUMINA-Bench further formalizes benchmarking protocols for single-topology training, multi-topology pretraining, held-out topology generalization, and transfer/adaptation, with unified metrics for prediction error and constraint violation [12]. Related LUMINA work also studies systematic generalization across coupled grid-optimization problems, including unit commitment (UC), security-constrained unit commitment (SCUC), AC-OPF, and unit-commitment AC optimal power flow (UC-ACOPF), where discrete commitment decisions and nonlinear AC power-flow feasibility must be satisfied jointly [13].

III. HETEROGENEOUS GRAPH LEARNING FOR OPTIMAL POWER FLOW

A. Heterogeneous Graph Representation of Power Grids

1) Node Types and Node Features

Each OPF instance is represented as a heterogeneous graph

$$\mathcal{G} = (\mathcal{V}, \mathcal{E}), \quad (1)$$

where the node set is decomposed into four typed subsets:

$$\mathcal{V} = \mathcal{V}_{\text{bus}} \cup \mathcal{V}_{\text{gen}} \cup \mathcal{V}_{\text{load}} \cup \mathcal{V}_{\text{shunt}}. \quad (2)$$

Table II summarizes the node types and their input-feature dimensions. The bus node is the target node type for the primary supervised task, while generators, loads, and shunts participate in message passing to inform bus-level predictions.

Bus features encode electrical state constraints and bus metadata, such as voltage limits, base voltage, and bus type.

TABLE I: Positioning of the proposed HydraGNN-based OPF workflow relative to prior GNN-based OPF surrogates and recent OPF graph foundation-model efforts.

Capability	Prior GNN and OPF-GFM Work	Proposed HydraGNN-Based Workflow
Graph representation	Early OPF-GNN surrogates often use homogeneous bus-branch graphs or architecture-specific encodings. Recent heterogeneous and LUMINA-style models explicitly represent multiple grid component types.	Preserves the native heterogeneous OPF structure in HydraGNN—buses, generators, loads, shunts, AC lines, transformers, and device-to-bus couplings—with node-type-specific embeddings and relation-specific message passing.
Architecture design	Many studies propose or benchmark a limited set of architectures. Recent OPF-GFM efforts compare homogeneous and heterogeneous backbones for topology transfer and feasibility-aware learning.	Integrates multiple heterogeneous backbones in one scalable workflow, spanning aggregation-, attention-, relational-attention-, transformer-, edge-aware, and degree-scaled operators.
Model-selection strategy	Prior work often uses manually selected architectures or benchmark-scale HPO. LUMINA-Bench includes matched HPO protocols across architectures and objectives at moderate scale.	Performs DeepHyper-driven, leadership-scale HPO on the full multi-case OPF corpus, enabling architecture selection under realistic large-data, distributed-training, and memory constraints.
Training scale	Most OPF surrogate studies target one topology or a small set of cases. Recent OPF-GFM benchmarks study multi-topology learning and transfer over selected OPFData cases.	Uses distributed preprocessing, sharded HDF5 storage, and multi-GPU training over the full ten-case corpus: approximately three million heterogeneous graphs spanning 14 to 13,659 buses.
Pretraining and fine-tuning	Recent OPF-GFM work has established multi-topology pretraining, zero-shot transfer, and fine-tuning/adaptation as important evaluation protocols.	Embeds pretraining and fine-tuning inside an end-to-end HydraGNN workflow, from full-corpus preprocessing and Frontier-scale HPO to downstream feasibility classification and $N-1$ contingency regression.
Response time	Learning-based surrogates provide fast inference, but many studies emphasize offline accuracy and feasibility metrics more than large-batch operational screening.	Targets low-latency inference for rapid screening of contingency, restoration, and operating-condition ensembles, reserving AC-OPF solves for selected high-risk or uncertain cases.
Physics awareness	Feasibility-aware OPF learning, including Lagrangian and augmented-Lagrangian objectives, penalizes power-balance, voltage, and line-flow violations; recent OPF-GFM benchmarks make feasibility central to evaluation.	Implements configurable OPF-domain penalties for voltage bounds, angle limits, and approximate thermal limits; large-scale HPO uses data-driven loss after preliminary penalties did not improve validation loss.
Systems and HPC contribution	Benchmark suites and OPF-GFM studies provide reproducible evaluation protocols and insight into topology transfer, feasibility, and adaptation.	Targets scalable OPF-GFM training through distributed HDF5 reuse, fault-tolerant HPO, Frontier-scale architecture comparison, and downstream model selection.
Smart-grid relevance	Prior work shows that GNN surrogates and OPF-GFM benchmarks can support faster OPF approximation and topology-transfer studies.	Frames heterogeneous OPF-GFM training as a scalable data-analytics capability for fast decision support in active, heterogeneous, and data-rich smart grids.

TABLE II: Node types and input-feature dimensions in the heterogeneous OPF graph.

Node Type	Input Dim.	Physical Meaning
bus	4	Electrical connection point and OPF state location
generator	11	Controllable power source connected to a bus
load	2	Active and reactive power demand
shunt	2	Reactive compensation device for voltage regulation

Generator features encode capacity limits, active and reactive power information, cost coefficients, current dispatch setpoints, and operating status. Load features encode active and reactive demand. Shunt features encode conductance and susceptance.

2) Edge Types and Edge Features

The edge set \mathcal{E} is the union of both physical electrical edges and structural equipment-to-bus links:

$$\mathcal{E} = \mathcal{E}_{ac} \cup \mathcal{E}_{tr} \cup \mathcal{E}_{gen} \cup \mathcal{E}_{load} \cup \mathcal{E}_{shunt}. \quad (3)$$

TABLE III: Typed edge relations in the heterogeneous OPF graph.

Source	Relation	Target	Physical Meaning
bus	ac_line	bus	AC line between buses
bus	transformer	bus	Transformer between buses
generator	generator_link	bus	Generator attached to bus
bus	generator_link	generator	Reverse generator link
load	load_link	bus	Load attached to bus
bus	load_link	load	Reverse load link
shunt	shunt_link	bus	Shunt attached to bus
bus	shunt_link	shunt	Reverse shunt link

Each edge relation is represented as a triplet consisting of source node type, edge type, and target node type. Table III lists the relations used in the heterogeneous OPF graph.

Only the two physical edge types carry continuous edge attributes, as summarized in Table IV. The structural links carry no continuous features but are included in both directions

TABLE IV: Edge-attribute dimensions in the heterogeneous OPF graph.

Edge Type	Has Attributes?	Feature Dim.
ac_line	Yes	9
transformer	Yes	11
generator_link	No	0
load_link	No	0
shunt_link	No	0

to enable bidirectional information flow between buses and attached equipment.

AC-line features describe electrical characteristics of a transmission line under a pi-equivalent model, including minimum and maximum angle difference, series resistance, series reactance, shunt susceptance terms, and thermal ratings. Transformer features include angle limits, series resistance, leakage reactance, off-nominal turns ratio, thermal ratings, tap setting, and phase shift. This distinction motivates heterogeneous architectures that can process relation-specific edge attributes with different dimensionalities.

IV. FULLY SUPERVISED OPF LEARNING TASK

A. OPF Surrogate Learning as a Smart-Grid Data-Analytics Task

In smart-grid applications, OPF surrogates are useful when many operating scenarios, topology perturbations, or control decisions must be evaluated quickly. Examples include real-time screening, contingency analysis, approximate dispatch, solver warm-starting, and rapid evaluation of operating-condition changes. In this paper, the learned model approximates the OPF solution map

$$f_* : \mathcal{X} \rightarrow \mathcal{Y}, \quad (4)$$

where \mathcal{X} denotes grid topology, component parameters, and operating context, and \mathcal{Y} denotes OPF solution quantities. The primary task considered in this paper is bus-level prediction of voltage angles and voltage magnitudes.

B. Input Features

The model input for one OPF sample is a heterogeneous graph

$$\mathcal{G} = (\{\mathbf{X}^\tau\}_{\tau \in \mathcal{T}_v}, \{\mathbf{E}^r, \mathbf{A}^r\}_{r \in \mathcal{T}_e}, \mathbf{g}), \quad (5)$$

where \mathbf{X}^τ is the node-feature matrix for node type τ , \mathbf{E}^r is the edge-index tensor for relation r , \mathbf{A}^r is the edge-attribute matrix when available, and \mathbf{g} denotes optional graph-level context features.

The input features include bus, generator, load, and shunt node features, AC-line and transformer edge attributes, and structural edge connectivity. For the primary bus-level prediction task, all node and edge types participate in message passing, but the decoder is applied only to bus-node embeddings.

C. Output Targets

The supervised target at each bus $i \in \mathcal{V}_{\text{bus}}$ is the two-vector $\mathbf{y}_i = [V_{a,i}, V_{m,i}]^\top$ of voltage angle (rad) and magnitude (p.u.), and the model outputs the corresponding prediction

$\hat{\mathbf{y}}_i = f_\Theta(\mathcal{G})_i$. The training objective is minimizing the bus-level mean squared error:

$$\mathcal{L}_{\text{sup}} = \frac{1}{|\mathcal{V}_{\text{bus}}|} \sum_{i \in \mathcal{V}_{\text{bus}}} \|\hat{\mathbf{y}}_i - \mathbf{y}_i\|_2^2. \quad (6)$$

All HPO trials in this work are trained with the purely data-driven supervised loss \mathcal{L}_{sup} defined above.

V. OPEN-SOURCE OPF DATASET

The dataset used in this work is the open-source PyTorch Geometric OPFDataset [21], which provides heterogeneous graph instances of solved AC-OPF problems derived from PGLib-OPF benchmark cases [22]. Each sample contains grid topology, component features, operating context, and OPF solution labels. The full dataset used for model selection contains ten PGLib-OPF cases spanning more than three orders of magnitude in grid size, from 14 to 13,659 buses: case14, case30, case57, and case118 (IEEE); case500, case2000, and case10000 (GOC); case4661 (SDET); case6470 (RTE); and case13659 (PEGASE). Each case contributes 300,000 independently drawn AC-OPF solutions, yielding a corpus of 3,000,000 heterogeneous graph instances in total. Using multiple cases is essential for the GFM objective: a model trained only on a single topology can learn topology-specific correlations, whereas training over many cases requires the model to learn reusable representations of grid structure, operating context, and component interactions.

VI. SCALABLE DATA PREPROCESSING AND HDF5 CONVERSION

The raw OPF data is converted into a format suitable for distributed training by selecting cases and splits, loading raw samples, constructing typed heterogeneous graph objects with node features, edge attributes, and bus-level OPF targets, attaching graph-level context, validating feature dimensions, and serializing the processed graphs into HDF5 shards.

The full OPF corpus contains approximately three million heterogeneous graph instances. Directly loading raw JSON files during every training run would impose significant I/O and preprocessing overhead. We therefore separate preprocessing from model training. Raw OPF samples are converted into typed heterogeneous graph objects and serialized into HydraGNN's HDF5 format. The full dataset is stored using 129 HDF5 shards, enabling scalable data access during distributed training and HPO. HDF5 conversion is essential for scalable HPO because each trial reuses the same processed dataset, avoiding repeated raw-data parsing, reducing filesystem pressure, and ensuring that all architecture comparisons use identical data.

VII. HYDRAGNN FRAMEWORK FOR SCALABLE HETEROGENEOUS OPF LEARNING

A. Extension from Homogeneous to Heterogeneous Graphs

HydraGNN provides scalable graph-learning infrastructure, including distributed training, configurable architectures, multi-head prediction, and high-performance data handling. The heterogeneous OPF branch extends HydraGNN from homogeneous graphs to heterogeneous graphs while preserving compatibility with existing homogeneous models.

The central abstraction is HeteroBase, which provides common infrastructure for all heterogeneous architectures. HeteroBase maintains separate input projectors for each node type, constructs relation-specific message-passing layers, supports variable edge-attribute dimensions, and decodes outputs on selected target node types.

B. Unique Features of HeteroBase

The heterogeneous extension introduces several capabilities important for OPF learning:

- **Per-node-type input embeddings:** separate linear projectors map bus, generator, load, and shunt features into a shared hidden space.
- **Per-edge-type message passing:** relation-specific convolution operators preserve the semantics of AC lines, transformers, and structural equipment links.
- **Variable edge-attribute dimensions:** physical edge types may carry different feature widths, e.g., nine for AC lines and eleven for transformers.
- **Featureless structural edges:** equipment-to-bus links can participate in message passing without continuous edge attributes.
- **Node-type-specific prediction:** all node types contribute to message passing, but the primary decoder is applied only to bus nodes.
- **Graph-level conditioning:** optional global context features can be injected through FiLM, node-level concatenation, or pooled fusion.
- **Multi-head decoding:** the framework supports future multi-task OPF learning with graph-level and node-level outputs.
- **Distributed-training compatibility:** eager metadata-based initialization ensures parameters are registered before distributed data parallel wrapping.

C. Supported Heterogeneous Architectures

The workflow supports a family of heterogeneous architectures summarized in Table V. This design treats the architecture as an experimental variable rather than a fixed modeling assumption.

HeteroSAGE builds on GraphSAGE mean aggregation [15]. HeteroGAT and HeteroRGAT build on graph-attention operators, using GATv2-style dynamic attention for HeteroGAT [17] and the original GAT-style attention mechanism for HeteroRGAT [16]. HeteroHGT uses the heterogeneous graph transformer operator, which introduces type-specific key, query, and value projections and relation-aware attention [19]. HeteroHEAT uses the heterogeneous edge-enhanced graph attention operator, which combines node-type information, edge-type embeddings, and continuous edge attributes [20]. HeteroPNA extends principal neighborhood aggregation [18] to heterogeneous bipartite relations through a wrapper that adapts PNAConv to source-target type pairs. In all cases, the HydraGNN contribution is not the invention of these base layers, but their integration into a common distributed heterogeneous OPF workflow with type-specific encoders, relation-specific message passing, scalable data loading, HPO, and downstream fine-tuning support.

D. Layer Provenance and HydraGNN New Contributions

The heterogeneous OPF models combine established graph-learning layers with new HydraGNN infrastructure. The base message-passing primitives are drawn from the literature: GraphSAGE for inductive neighborhood aggregation, GAT and GATv2 for attention-based message passing, PNA for multi-aggregator degree-scaled message passing, HGT for type-aware graph-transformer attention, and HEAT for edge-attribute-aware heterogeneous attention. In addition to the features mentioned in section VII-A, HydraGNN provides node-type-specific feature projections, relation-specific layer construction, support for variable edge-attribute dimensions, bus-level target decoding, OPF-domain regularization, HDF5-based distributed data loading, and Frontier-scale HPO across all candidate architectures.

VIII. SCALABLE HYPERPARAMETER OPTIMIZATION

A. DeepHyper-Based HPO

To identify architectures and hyperparameters suitable for full-dataset OPF surrogate modeling, we performed HPO using DeepHyper Centralized Bayesian Optimization with an Upper Confidence Bound acquisition function. The search space is summarized in Table VI.

We launched six architecture-specific HPO runs, one per GNN architecture (HeteroSAGE, HeteroHEAT, HeteroHGT, HeteroPNA, HeteroRGAT, and HeteroGAT). Fixing the architecture within each HPO run allows the optimizer to search the continuous and integer hyperparameters under the same compute budget and data distribution.

B. Frontier Execution Strategy

The full-dataset HPO campaign was executed on the ORNL Frontier supercomputer. Each architecture-specific HPO run used 512 Frontier nodes, corresponding to 4,096 AMD MI250X GPUs. Each trial used 32 nodes, or 256 GPUs, enabling 16 concurrent trials per HPO run per GNN architecture. Each trial trained for 10 epochs with batch size 32 and a 6-hour wall-time limit per HPO run.

The minimum validation loss across completed epochs was used as the HPO objective rather than the final-epoch loss. This is important because some architectures exhibit oscillatory training or early overfitting, and the best validation loss provides a more robust measure of trial quality.

C. Fault Tolerance and Result Reuse

At this scale, individual configurations can fail from out-of-memory errors, communication instability, or model-specific limitations. The HPO framework isolates trial-level failures so that one failed trial does not interrupt the campaign; if a trial is terminated early, the best validation loss from its completed epochs is recovered when available. Results are saved in a CSV file and can warm-start follow-up searches. Completion rates vary widely across architectures, from 50% for HeteroSAGE and HeteroHEAT to $\approx 75\%$ for HeteroRGAT, $\approx 21\%$ for HeteroHGT, and under 2% for HeteroPNA; valid-trial counts appear on the x-axis of Figure 1.

TABLE V: Heterogeneous architectures supported by the HydraGNN OPF workflow.

Model	Layer Type	Uses Edge Attributes?	Key Feature
HeteroSAGE	SAGEConv per relation	No	Stable mean aggregation with type separation
HeteroGAT	GATv2Conv per relation	Yes	Dynamic attention per relation
HeteroRGAT	GATConv per relation	Yes	Relation-specific graph attention
HeteroHGT	HGTConv	No	Type-specific key/query/value projections
HeteroHEAT	HEATConv	Yes	Type-aware and edge-attribute-aware attention
HeteroPNA	PNACConv with bipartite wrapper	Yes	Multi-aggregator degree-scaled message passing

TABLE VI: Hyperparameter search space for full-dataset HPO.

Hyperparameter	Range	Type
hidden_dim	[32, 256]	Integer
num_conv_layers	[2, 6]	Integer
learning_rate	$[10^{-5}, 10^{-2}]$	Log-uniform
mpnn_type	fixed per HPO run	Categorical

IX. RESULTS: ARCHITECTURE EVALUATION, OPF GFM PRE-TRAINING AND FINE-TUNING PROTOCOLS

A. Full-Dataset HPO Results

The full HPO campaign dispatched 387 trials across six architectures and produced 153 valid trials (DONE status with a recorded objective). Figure 1 visualizes the trial-level distributions per architecture, with valid/dispatched counts on the x-axis and the best trial marked. All results use the full ten-case dataset rather than single-case screening.

B. Architecture Ranking and Interpretation

Figure 1 shows the per-trial validation-loss distributions as box plots with overlaid points and starred best trials, capturing both peak performance and typical behavior across the search space. Figure 2 complements this view by plotting validation loss against trainable parameter count: HeteroSAGE ($\sim 1.6M$ params) and HeteroHEAT ($\sim 1.7M$) reach the lowest losses at substantially smaller model sizes than HeteroRGAT ($\sim 3.5M$), HeteroHGT ($\sim 3.2M$), and HeteroGAT ($\sim 3.2M$), none of which match the top tier even at much larger budgets. *Crucially, the HPO results reveal no evident correlation between model accuracy and model size: larger parameter counts do not systematically yield lower validation losses, and the best-performing architectures are among the most compact.*

Leading architectures: HeteroSAGE and HeteroHEAT.

HeteroSAGE and HeteroHEAT achieve essentially identical best validation losses, suggesting both have reached a similar accuracy ceiling within the 10-epoch HPO budget. Both also have the lowest median validation losses, with only a small gap between them (Figure 1), confirming that their superiority is not a single-trial artifact.

Sensitivity to hyperparameters. Despite comparable peak and median performance, HeteroSAGE and HeteroHEAT differ in hyperparameter sensitivity, as measured by the cross-trial spread (Figure 1). HeteroHEAT has a noticeably wider distribution, indicating greater sensitivity to hidden dimension, depth, and learning rate. This matches the architectural difference: simple mean aggregation in HeteroSAGE is inherently stable, while the type- and edge-aware attention in Hetero-

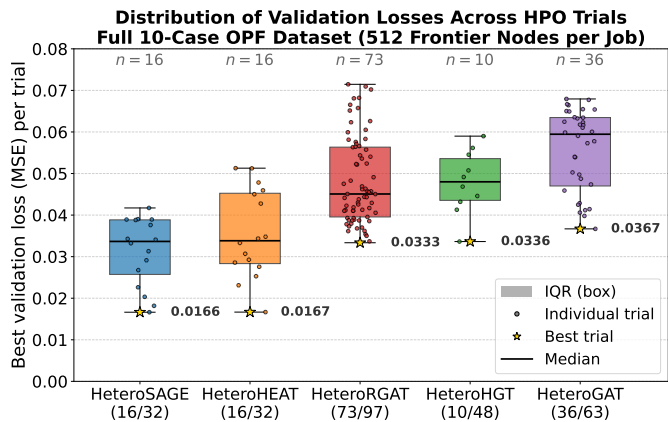


Fig. 1: Distribution of per-trial best validation losses across HPO trials for each architecture (HeteroPNA excluded: only two valid trials out of 115 dispatched). X-axis labels report architecture name and valid/dispatched trial counts. Boxes span the 25th–75th percentile; whiskers extend to $1.5\times$ the interquartile range; jittered points overlay individual trials; gold stars mark the best trial per architecture.

HEAT can amplify or suppress information depending on the learning dynamics. For deployment, HeteroSAGE is the more robust default; HeteroHEAT reaches comparable accuracy but needs more careful tuning.

Second-tier architectures. HeteroRGAT (73 valid trials) and HeteroHGT (10 valid trials) form a second tier, with best validation losses roughly twice those of the leaders (Figure 1). They are essentially tied on best loss but differ in spread: HeteroHGT is more concentrated around its mean, though its low completion rate limits confidence in the comparison and suggests that many configurations exhaust resources before producing reliable results. HeteroGAT performs worst among the architectures with a usable trial set; its median exceeds its mean, so most trials underperform the average and the best value is an outlier.

HeteroPNA stability issues. HeteroPNA produced only two valid trials out of 115 dispatched (under 2% completion), attributable to the bipartite PNA wrapper used to extend PNAConv to heterogeneous graphs, which imposes higher memory and communication overhead at 256 GPUs per trial. The two surviving trials nominally place HeteroPNA between the top and second tiers, but reflect an extreme selection effect—only the easiest (likely smallest hidden dimension) configurations succeeded—so no reliable mean, standard deviation, or median can be reported.

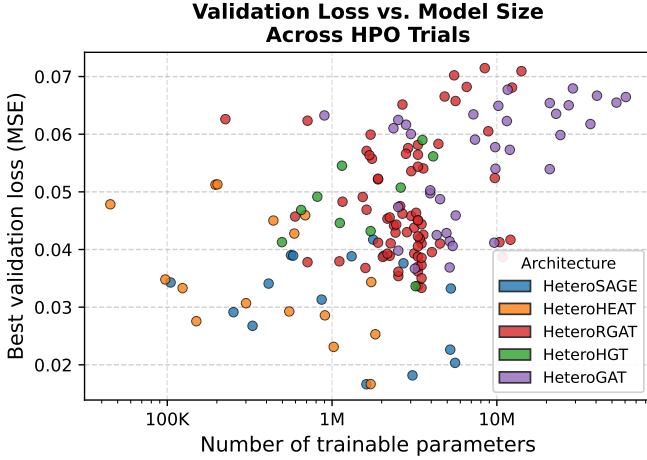


Fig. 2: Validation loss vs. number of trainable parameters per HPO trial on a log scale, colored by architecture.

C. Model Selection for Subsequent Experiments

Based on the full-dataset HPO campaign, we select HeteroSAGE and HeteroHEAT as the primary architectures for subsequent pretraining and fine-tuning. HeteroSAGE is the default scalable baseline: it attains the best validation loss with the lowest cross-trial spread (Figure 1), so its advantage is robust to hyperparameter variation rather than tied to a narrow region of the search space. HeteroHEAT is the edge-aware attention alternative, with comparable peak accuracy and median while explicitly leveraging continuous edge attributes and type embeddings. HeteroRGAT and HeteroHGT are retained as secondary baselines, since their distinct architectural families (relational attention and type-aware transformer) may behave differently under topology-specific fine-tuning. HeteroGAT shows consistently higher losses and an unfavorable median-to-mean ratio, indicating limited suitability for the full-scale task.

D. Pretraining Across OPF Cases

The model is exposed to a broad collection of OPF cases spanning different network sizes, demand profiles, generation mixes, operating constraints, renewable-penetration levels, and topology perturbations. This forces the heterogeneous encoder to learn reusable representations of power-system structure and physics, rather than correlations that are specific to one benchmark case. In particular, the encoder learns how typed grid components—buses, generators, loads, shunts, transmission lines, transformers, and device-to-bus couplings—jointly determine OPF solution quantities such as voltage magnitudes and voltage angles.

Let

$$\mathcal{D}_{\text{pre}} = \{\mathcal{D}_1, \dots, \mathcal{D}_K\} \quad (7)$$

denote the collection of datasets used for pretraining, where each \mathcal{D}_k corresponds to one OPF case, grid family, or operating regime. Each sample in \mathcal{D}_k is a pair $(\mathcal{G}, \mathbf{y})$, where \mathcal{G} is the heterogeneous graph representation of the power-grid instance and \mathbf{y} contains the supervised OPF targets. As mentioned before, in this work, the primary targets are bus-level voltage angles and voltage magnitudes.

The model is written as

$$\hat{\mathbf{y}} = f_{\Theta_{\text{enc}}, \Theta_{\text{head}}}(\mathcal{G}), \quad (8)$$

where Θ_{enc} denotes the parameters of the heterogeneous graph encoder and Θ_{head} denotes the parameters of the task-specific prediction head. The supervised loss \mathcal{L}_{sup} measures the discrepancy between the model prediction $\hat{\mathbf{y}}$ and the OPF target \mathbf{y} ; for example, for bus-level voltage prediction it can be defined as a mean-squared error over the predicted voltage angles and magnitudes.

The pretraining objective is therefore

$$\min_{\Theta_{\text{enc}}, \Theta_{\text{head}}} \sum_{k=1}^K \mathbb{E}_{(\mathcal{G}, \mathbf{y}) \sim \mathcal{D}_k} [\mathcal{L}_{\text{sup}}(f_{\Theta_{\text{enc}}, \Theta_{\text{head}}}(\mathcal{G}), \mathbf{y})]. \quad (9)$$

This objective trains a single encoder over all pretraining cases. The resulting model can then be used as an initialization for downstream OPF tasks, where the amount of labeled high-fidelity data may be much smaller.

Realizing this representation quality at scale requires leadership-class infrastructure. Large OPF datasets contain millions of heterogeneous graph instances once scenario, topology, and uncertainty dimensions are considered, demanding distributed data loading, scalable batching, and parallel training across thousands of GPUs.

E. Fine-Tuning on Target Grid Cases

The second defining feature of a successful GFM paradigm is rapid and accurate fine-tuning. After pretraining, the encoder is adapted to high-value downstream OPF settings, such as specific planning regions, large-load integration studies, renewable and storage deployment scenarios, contingency analysis, or coupled transmission-distribution studies. In these settings, high-fidelity OPF data may be expensive to generate. Fine-tuning specializes the pretrained model to the target topology, constraints, and operating regime while requiring fewer labeled OPF solutions than training a topology-specific surrogate from scratch.

Let \mathcal{D}_{ft} denote the target fine-tuning dataset. The trainable parameter set is denoted by Θ_{ft} . Depending on the amount of target data available, Θ_{ft} may include all model parameters, only the prediction head, or the prediction head together with the final message-passing layers. This allows the same pretrained model to support multiple adaptation regimes.

F. Fine-Tuning Scenarios

The proposed workflow supports several fine-tuning scenarios:

- **Topology-specific fine-tuning:** pretrain on several OPF cases and fine-tune on a target grid topology with limited labeled OPF solutions.
- **Operating-condition fine-tuning:** pretrain on broad operating regimes and fine-tune on new load, generation, or renewable-penetration scenarios.
- **Contingency fine-tuning:** pretrain on nominal conditions and fine-tune on topology perturbations or $N - 1$ contingency scenarios.
- **Task-specific fine-tuning:** pretrain on bus-voltage prediction and fine-tune for related OPF quantities, such as generator dispatch, line-flow prediction, or feasibility classification.

G. Fine-Tuning Experimental Setup

Two downstream experiments quantify the benefit of pretraining versus training from scratch as a function of labeled data volume.

FT1 is binary feasibility classification: predict whether the AC-OPF solution underlying a given OPF graph instance is feasible. The FT1 dataset is generated entirely from existing OPF data without additional solver calls. Feasible samples are drawn directly from the open-source OPFDataset [21] for the IEEE 118-bus case (`pglib_opf_case118_ieee`). Infeasible samples are synthesised by scaling all load features (active and reactive demand, P_d and Q_d) by a factor of 6, which guarantees that total demand exceeds total generation capacity. The result is a balanced dataset (50% feasible, 50% infeasible). The pretrained regression head is replaced by a binary graph-level head trained with binary cross-entropy (BCE); test metrics are accuracy, F1, and AUC-ROC.

FT2 is $N-1$ contingency regression: given a single-line outage, predict bus voltage angles (V_a) and magnitudes (V_m); the test metric is MSE per quantity. The FT2 dataset is retrieved directly from the same open-source OPFDataset [21] for the IEEE 118-bus case, using the dataset’s built-in topological-perturbation support, which provides solved AC-OPF instances under single-line outage scenarios without requiring any additional data generation.

Both experiments compare four adaptation regimes applied to the pretrained HeteroSAGE and HeteroHEAT models from Section IX:

- **Full fine-tuning (FT-F):** all parameters updated.
- **Partial fine-tuning (FT-P):** head and final message-passing layer updated; earlier layers frozen.
- **Head-only fine-tuning (FT-H):** only the head updated.
- **Scratch (SCR):** random initialization with the same architecture and training budget.

Labeled sample sizes range from $n = 100$ to $n = 50,000$ for both tasks. All runs train for 50 epochs at learning rate 10^{-4} on 8 Frontier nodes (64 AMD MI250X GPUs).

H. FT1: OPF Feasibility Classification

The feasibility task is rapidly saturated in terms of validation accuracy: nearly all regime–architecture combinations reach perfect classification at the smallest sample size. This indicates that the GFM encoder, pretrained on multi-case AC-OPF solutions, has already learned a latent space in which feasible and infeasible operating points are well separated, so a small labeled head suffices to recover the decision boundary. The few exceptions collapse to a degenerate all-positive predictor, consistent with the class imbalance of the dataset. Partial fine-tuning (head plus final message-passing layer) avoids this failure for both architectures, showing that a single round of message-passing adaptation aligns the encoder with the downstream label distribution while preserving the pretrained geometry. Although validation accuracy saturates to near-perfect for most regime–architecture combinations already at $n = 100$, the validation BCE loss shown in Figure 3 reveals a persistent gap between adaptation regimes, where fine-tuning reaches substantially lower loss than scratch training and converges faster, with the difference most pronounced at

small n . This shows that the pretrained representation yields better-calibrated predictions even when accuracy alone cannot distinguish the regimes.

It is also worth noting that, at large n , head-only fine-tuning falls behind partial and full FT in validation BCE. The underlying reason is that the pretrained encoder was trained on bus-voltage regression, so its internal representations are shaped to minimize MSE for regression tasks, rather than producing well-calibrated classification probabilities. At small n the task is easy enough that a linear head can find a decision boundary in those regression-oriented features. As the labeled dataset grows, partial and full FT have enough signal to update the encoder itself, re-orienting its representations toward the classification objective, while head-only FT remains locked to features that were never trained for this purpose, causing its BCE to stall or worsen relative to the other regimes.

I. FT2: $N-1$ Contingency OPF Regression

The $N-1$ contingency regression task is substantially more demanding than FT1 and provides a clearer test of whether pretraining improves downstream adaptation. Figure 4 shows four complementary benefits of fine-tuning a pretrained OPF GFM instead of training the same architecture from scratch.

First, fine-tuning improves accuracy in the low-data regime. At small sample sizes, partial fine-tuning consistently reaches lower validation MSE than scratch training for both HeteroSAGE and HeteroHEAT. This indicates that the pretrained encoder already contains reusable information about the relationship between grid topology, component attributes, and bus-level voltage states, so the downstream model does not need to relearn these representations from a limited contingency dataset.

Second, fine-tuning stabilizes training. Scratch training and full fine-tuning exhibit larger oscillations in the validation loss, especially at the smallest sample sizes, whereas partial fine-tuning produces smoother convergence. This behavior suggests that the pretrained GFM acts as an inductive bias: freezing the early message-passing layers constrains the adaptation dynamics and reduces the tendency of the model to overreact to small downstream batches.

Third, fine-tuning accelerates convergence even when more labeled downstream data are available. Across the evaluated sample sizes, partial and head-only fine-tuning reach their best attainable validation losses in fewer epochs than scratch training. Thus, the advantage of the GFM is not limited to small-data accuracy; it also reduces the number of optimization steps required to adapt the model to the downstream contingency-regression task.

Fourth, partial and head-only fine-tuning reduce computational cost because only a subset of the model parameters is updated. This reduces the amount of gradient computation and optimizer-state storage relative to full fine-tuning or scratch training. In the present experiments, partial and head-only fine-tuning complete reliably within the 8-node (64 AMD MI250X GPU) wall-time budget, whereas full fine-tuning and scratch training are slower and less stable.

Taken together, the FT2 results show that, for the $N-1$ contingency regression task, partial fine-tuning provides the best trade-off among accuracy, stability, convergence speed,

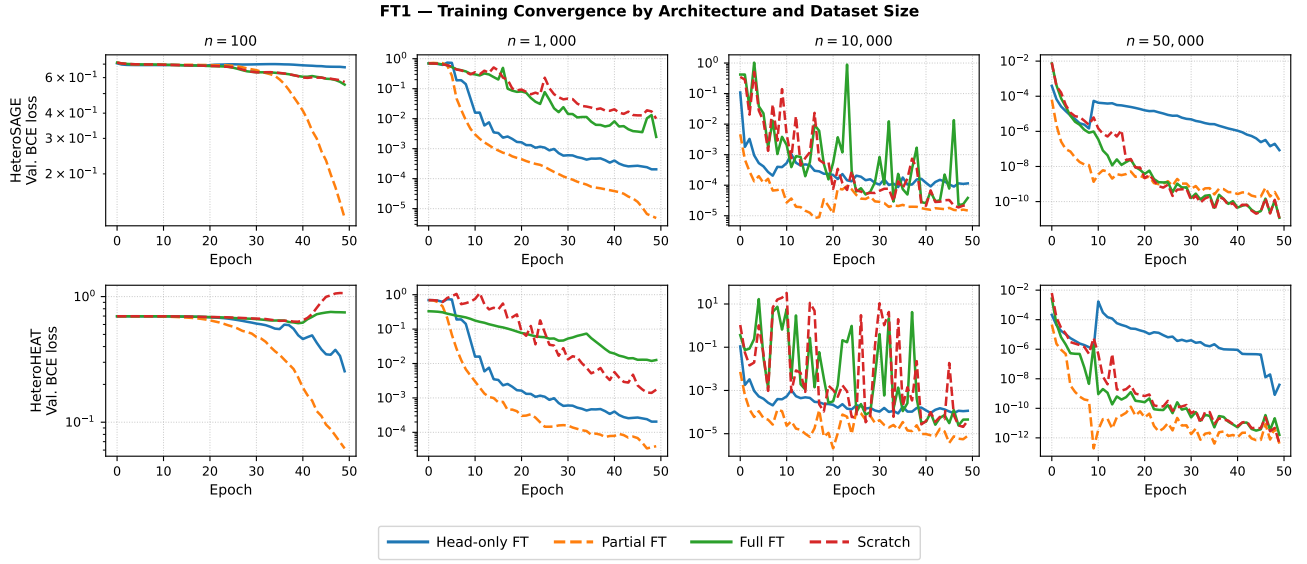


Fig. 3: FT1 feasibility classification: validation BCE loss vs. training epoch for HeteroSAGE (top row) and HeteroHEAT (bottom row) at four sample sizes.

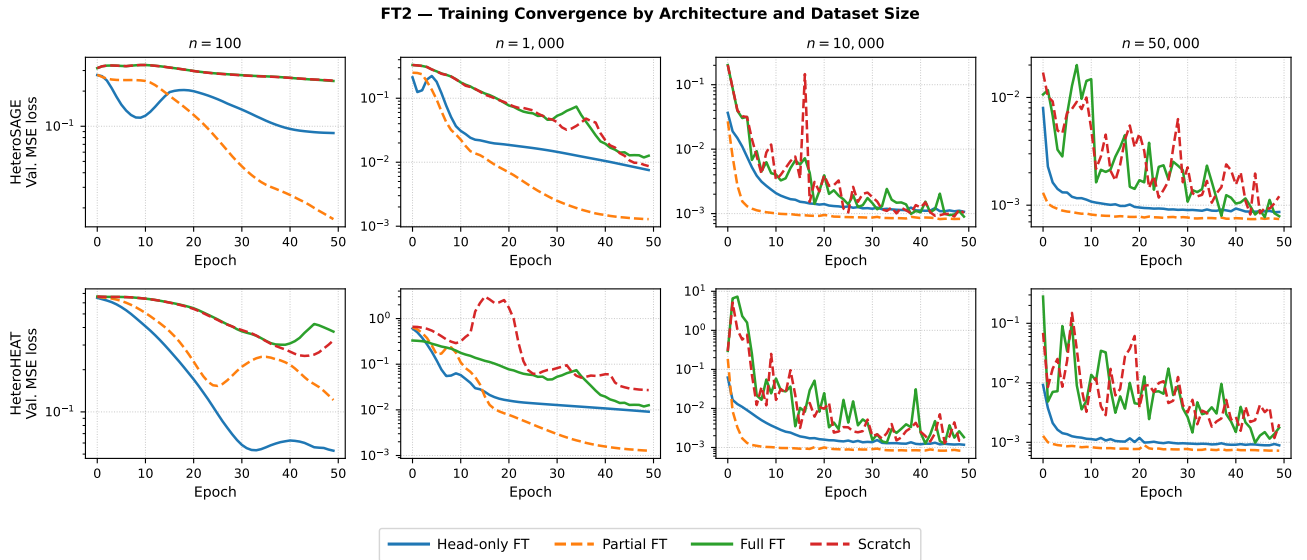


Fig. 4: FT2 $N-1$ contingency regression: validation MSE loss versus training epoch for HeteroSAGE and HeteroHEAT across multiple labeled-data regimes.

and computational cost. Full fine-tuning is less reliable because unconstrained updates to all layers can overwrite useful pretrained representations, consistent with catastrophic forgetting [23], and should be reserved for cases where the downstream dataset is large and the shift from pretraining is substantial. Head-only fine-tuning is computationally cheapest and stable, but it can be less accurate than partial fine-tuning when the downstream task requires some adaptation of the message-passing representation.

X. CONCLUSION

This paper presented a scalable HydraGNN workflow for developing, pretraining, selecting, and fine-tuning heterogeneous OPF GfMs over the full multi-case OPF corpus using

leadership-class computing.

First, we extended HydraGNN with heterogeneous graph learning support for OPF, including node-type-specific embeddings, relation-specific message passing, variable edge-attribute handling, heterogeneous pooling, graph-level conditioning, and bus-level prediction heads. This enables the model to preserve the physical semantics of buses, generators, loads, shunts, AC lines, transformers, and device-to-bus couplings within a scalable distributed graph-learning framework.

Second, we developed a full-corpus distributed training and model-selection workflow. Approximately three million heterogeneous graph instances from ten PGLib-OPF cases, spanning 14 to 13,659 buses, were converted into sharded HDF5 datasets and used for DeepHyper-driven HPO on the

ORNL Frontier supercomputer. The campaign produced 153 valid trials across six heterogeneous GNN architectures and identified HeteroSAGE and HeteroHEAT as the leading models. These architectures achieved the lowest validation losses—roughly half those of the next-best architectures—while remaining compact, with no evidence that larger parameter counts systematically improved accuracy.

Third, we evaluated the downstream value of the pretrained OPF GFM through fine-tuning on OPF feasibility classification and $N-1$ contingency regression. The feasibility task showed that the pretrained representation can provide highly data-efficient classification, while the contingency-regression task showed that partial fine-tuning achieves lower validation MSE and more stable convergence than scratch training in the small-data regime. Full fine-tuning was slower and less stable, consistent with catastrophic forgetting of the pretrained representation. Together, these results support the GFM paradigm: multi-case pretraining amortizes representation learning across grid families, and targeted fine-tuning improves data efficiency, training stability, and computational cost on downstream OPF tasks.

Future work will evaluate per-topology transfer and held-out-topology generalization, validate the framework on real-world utility data, and integrate time-series operating conditions with solver-in-the-loop verification for real-time grid decision support and resilience analysis.

REFERENCES

- [1] M. B. Cain, R. P. O'Neill, and A. Castillo, "History of optimal power flow and formulations," Federal Energy Regulatory Commission (FERC), Tech. Rep., 2012.
- [2] S. Frank, I. Steponavice, and S. Rebennack, "Optimal power flow: A bibliographic survey I – formulations and deterministic methods," *Energy Systems*, vol. 3, no. 3, pp. 221–258, 2012.
- [3] D. Owerko, F. Gama, and A. Ribeiro, "Optimal power flow using graph neural networks," *arXiv preprint arXiv:1910.09658*, 2019.
- [4] S. Liu, C. Wu, and H. Zhu, "Topology-aware graph neural networks for learning feasible and adaptive ac-opf solutions," *IEEE Transactions on Power Systems*, 2023.
- [5] Z. Guo, K. Sun, B. Park, S. Simunovic, and W. Kang, "A directed acyclic graph neural network for ac optimal power flow," in *2023 IEEE Power & Energy Society General Meeting (PESGM)*, 2023.
- [6] A. Deihim, D. Apostolopoulou, and E. Alonso, "Initial estimate of ac optimal power flow with graph neural networks," *Electric Power Systems Research*, vol. 234, p. 110782, 2024.
- [7] F. Fioretto, T. W. K. Mak, and P. Van Hentenryck, "Physics-informed neural networks for ac optimal power flow," *Electric Power Systems Research*, vol. 212, p. 108412, 2022.
- [8] S. Ghamizi, A. Ma, J. Cao, and P. Rodriguez Cortes, "OPF-HGNN: Generalizable heterogeneous graph neural networks for ac optimal power flow," in *2024 IEEE Power & Energy Society General Meeting (PESGM)*, 2024.
- [9] A. Triguí, M. Olama, G. Siopsis, H. Eldakhkhni, and M. Salhi, "Graph-based attention mechanisms for solving the ac optimal power flow problem in electrical power networks," in *2025 57th North American Power Symposium (NAPS)*, 2025.
- [10] A. Wen, B. Wen, J. Li, and J. Xu, "Heterogeneous graph neural network with local and global message passing for ac-optimal power flow solutions," *Applied System Innovation*, vol. 9, no. 1, p. 18, 2026.
- [11] Y. Li, Z. Memon, H. Jin, S. Fenu, K. Song, S. B. Sharma, P. Gasana, H. Kim, L. Zhao, and K. Kim, "LUMINA: Foundation models for topology transferable ACOPT," in *International Conference on Learning Representations (ICLR)*, 2026, arXiv:2603.04300. [Online]. Available: <https://arxiv.org/abs/2603.04300>
- [12] H. Jin, K. Song, Z. Memon, Y. Li, S. Fenu, H. Kim, L. Zhao, and K. Kim, "LUMINA: A grid foundation model for benchmarking AC optimal power flow surrogate learning," *arXiv preprint arXiv:2605.02133*, 2026. [Online]. Available: <https://arxiv.org/abs/2605.02133>
- [13] Z. Memon, Y. Li, H. Jin, K. Kim, and L. Zhao, "Towards systematic generalization for power grid optimization problems," *arXiv preprint arXiv:2605.02026*, 2026. [Online]. Available: <https://arxiv.org/abs/2605.02026>
- [14] M. Lupo Pasini, S. T. Reeve, P. Zhang, and J. Y. Choi, "HydraGNN," Distributed PyTorch implementation of multi-headed graph convolutional neural networks, United States, Oct. 2021. [Online]. Available: <https://www.osti.gov/biblio/code-65891>
- [15] W. L. Hamilton, R. Ying, and J. Leskovec, "Inductive representation learning on large graphs," in *Advances in Neural Information Processing Systems*, 2017.
- [16] P. Veličković, G. Cucurull, A. Casanova, A. Romero, P. Liò, and Y. Bengio, "Graph attention networks," in *International Conference on Learning Representations*, 2018.
- [17] S. Brody, U. Alon, and E. Yahav, "How attentive are graph attention networks?" in *International Conference on Learning Representations*, 2022.
- [18] G. Corso, L. Cavalleri, D. Beaini, P. Liò, and P. Veličković, "Principal neighbourhood aggregation for graph nets," in *Advances in Neural Information Processing Systems*, vol. 33, 2020, pp. 13 260–13 271.
- [19] Z. Hu, Y. Dong, K. Wang, and Y. Sun, "Heterogeneous graph transformer," in *Proceedings of The Web Conference 2020*, 2020, pp. 2704–2710.
- [20] X. Mo, Y. Xing, and C. Lv, "Heterogeneous edge-enhanced graph attention network for multi-agent trajectory prediction," *arXiv preprint arXiv:2106.07161*, 2021.
- [21] T. Lovett, A. Buovich, A. Sharma, S. Pegg, S. Cohen, S. Stephens, A. Tucker, P. Pope, J. Eiselen, F. Buchaca, C. Sutton, J. Mantilla-Bilbao, T. Roeder, Y. Lin, E. Bridgett-Tomkinson, J. Garratt, J. Patterson, S. Lyons, A. Hales, and V. Petar, "OPFData: Large-scale datasets for machine learning-accelerated ac optimal power flow," *arXiv preprint arXiv:2406.07234*, 2024.
- [22] S. Babaeinejadsarookolae, A. Birchfield, R. D. Christie, C. Coffrin, C. DeMarco, R. Diao, M. Ferris, S. Fliscounakis, S. Greene, C. Jozs, R. Korab, B. Lesieutre, J. Maeght, D. K. Molzahn, T. J. Overbye, P. Panciatici, B. Park, J. Snodgrass, A. Tbaileh, and R. D. Zimmerman, "The power grid library for benchmarking ac optimal power flow algorithms," *arXiv preprint arXiv:1908.02788*, 2019.
- [23] J. Kirkpatrick, R. Pascanu, N. Rabinowitz, J. Veness, G. Desjardins, A. A. Rusu, K. Milan, J. Quan, T. Ramalho, A. Grabska-Barwinska, D. Hassabis, C. Clopath, D. Kumaran, and R. Hadsell, "Overcoming catastrophic forgetting in neural networks," *Proceedings of the National Academy of Sciences*, vol. 114, no. 13, pp. 3521–3526, 2017.